



# Thermodynamic constraints on the formation of condensed carbon from serpentization fluids

Vincent Milesi, Thomas M Mccollom, François Guyot

## ► To cite this version:

Vincent Milesi, Thomas M Mccollom, François Guyot. Thermodynamic constraints on the formation of condensed carbon from serpentization fluids. *Geochimica et Cosmochimica Acta*, 2016, 189, pp.391-403. 10.1016/j.gca.2016.06.006 . hal-04755670

**HAL Id: hal-04755670**

**<https://hal.science/hal-04755670v1>**

Submitted on 28 Oct 2024

**HAL** is a multi-disciplinary open access archive for the deposit and dissemination of scientific research documents, whether they are published or not. The documents may come from teaching and research institutions in France or abroad, or from public or private research centers.

L'archive ouverte pluridisciplinaire **HAL**, est destinée au dépôt et à la diffusion de documents scientifiques de niveau recherche, publiés ou non, émanant des établissements d'enseignement et de recherche français ou étrangers, des laboratoires publics ou privés.

**THERMODYNAMIC CONSTRAINTS ON THE FORMATION OF CONDENSED  
CARBON FROM SERPENTINIZATION FLUIDS**

**Vincent Milesi <sup>a,\*</sup>, Thomas M. McCollom <sup>b</sup> and François Guyot <sup>c</sup>**

<sup>a</sup> Équipe de Géochimie des Eaux,  
Institut de Physique du Globe de Paris,  
Sorbonne Paris Cité,  
Université Paris Diderot,  
UMR CNRS 7154,  
F-75005 Paris, France.

<sup>b</sup> Laboratory for Atmospheric and Space Physics  
University of Colorado  
Boulder, Colorado 80309, USA

<sup>c</sup> Institut de minéralogie et de physique des matériaux et de cosmochimie,  
Sorbonne Université. Muséum National d'Histoire Naturelle,  
UMR 7590, CNRS, UPMC, MNHN, IRD,  
F-75005 Paris, France.

20

21     \* Corresponding author:

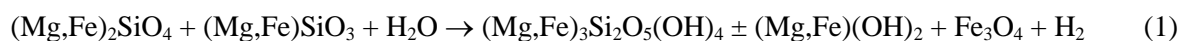
22     *E-mail address:* [milesi@ipgp.fr](mailto:milesi@ipgp.fr) (Vincent Milesi)

24       Recent studies have identified carbonaceous material in serpentinite bodies, but  
25 whether these deposits have a biologic or abiotic origin remains uncertain. In this work,  
26 thermodynamic calculations were performed to examine the potential for abiotic condensed  
27 carbonaceous material to be produced from serpentinization-derived fluids under  
28 hydrothermal conditions. Calculation of reaction pathways during serpentinization of olivine  
29 showed that fluid compositions should equilibrate with condensed carbonaceous material,  
30 which controls the H<sub>2</sub> and CO<sub>2</sub> activities. Fluids from laboratory serpentinization experiments  
31 and from the Lost City and the Rainbow hydrothermal field are shown to be consistent with  
32 this model. The predictions indicate that carbonaceous material should be the dominant  
33 carbon product of CO<sub>2</sub> reduction in these hydrothermal settings, which would have significant  
34 implications for a number of processes, including the deep Earth carbon cycle by creating a  
35 pool of relatively immobile reduced carbon, the extent of H<sub>2</sub> production in ultrabasic  
36 environments, and mechanisms leading to abiotic reduced carbon compounds.

# 1. INTRODUCTION

It is widely recognized that the serpentinization of ultramafic rocks creates strongly reducing conditions that are favorable for abiotic reduction of inorganic carbon. Indeed, there is mounting evidence that fluids discharged from actively serpentinizing systems contain methane, formate and other simple organic compounds formed by abiotic carbon reduction within these systems (Charlou et al., 2002, 2010; Proskurowski et al., 2008; Lang et al., 2010; Etiope et al., 2013a, 2013b; Etiope and Sherwood Lollar, 2013; McDermott et al., 2015). In addition, a number of laboratory studies have demonstrated that methane and other small organic compounds can be generated from reduction of inorganic carbon at conditions simulating those of hydrothermal serpentinization fluids (Berndt et al., 1996; Horita and Berndt, 1999; McCollom and Seewald, 2001, 2003; Foustoukos and Seyfried, 2004; Seewald et al., 2006; Fu et al., 2007).

In general terms, the serpentinization of ultramafic rocks can be represented by the reaction:



olivine      orthopyroxene                      serpentine                      brucite      magnetite

The generation of  $\text{H}_2$  during this process results from oxidation of ferrous iron ( $\text{Fe}^{\text{II}}$ ) released by the primary minerals through reaction with  $\text{H}_2\text{O}$ , producing ferric iron ( $\text{Fe}^{\text{III}}$ ) that precipitates in magnetite or serpentine. The formation of methane and other organic compounds is generally thought to proceed from reduction of inorganic carbon by the  $\text{H}_2$  generated by Rxn. 1, which can be expressed in general as:



methane      ethane      formic acid

While the evidence for abiotic generation of small organic compounds during serpentinization has gotten stronger over the last couple of decades, it has remained uncertain whether carbon reduction extends to more complex compounds. Holm and Charlou (2001) observed long-chain hydrocarbons ( $C_{16}$  -  $C_{29}$ ) in extracts of hydrothermal fluids from the ultramafic-hosted Rainbow system on the Mid-Atlantic Ridge (MAR) which they inferred were derived from abiotic reduction of inorganic carbon by Fischer-Tropsch-type (FTT) processes. However, subsequent studies have not found any definitive evidence for long-chain hydrocarbons or other high-molecular-weight organic compounds with an abiotic origin at Rainbow or at other ultramafic-hosted sites on the MAR (Konn et al., 2009, 2012; McCollom et al., 2015). Delacour et al. (2008) identified a number of long-chain linear alkanes resembling those produced by FTT reactions in serpentinized rocks recovered near the Lost City hydrothermal field. However, the presence of biomarker compounds such as pristane and phytane indicated that there was a substantial contribution of biologically derived organic matter to the rocks, making evaluations of a possible abiotic source for the alkanes equivocal. In samples of deep altered oceanic crust, Shilobreeva et al. (2011) measured bulk carbon with a heavy isotopic composition that they explained as a mixture between carbonate and organic compounds produced from the abiotic reduction of magmatic  $CO_2$ . Recent studies by Ménez et al. (2012) and Pasini et al. (2013) identified macromolecular carbon deposits in serpentinites recovered from the seafloor, which were interpreted to be ultimately derived from biological organisms. Over the years, several studies reported the occurrence of graphite associated with serpentinites (e.g., Krishnarao, 1964; Chidester, 1978; Pasteris, 1981, 1988; Luque et al., 1992, 1998; Miura et al., 2011; Galvez et al., 2013; Kawamoto et al., 2013). Although it has been suggested that these graphite deposits precipitated from reduction of  $CO_2$  transported into the rocks by hydrothermal fluids, it remains undetermined how they actually formed.

A number of laboratory experimental studies have been performed to examine inorganic carbon reduction during serpentinization. However, these studies have predominantly focused on formation of CH<sub>4</sub> and light hydrocarbons (e.g., Berndt et al., 1996; Horita and Berndt, 1999; McCollom and Seewald, 2001, 2003; Foutoukos and Seyfried, 2004; Fu et al., 2007). In some of these studies, mass balance calculations indicate decreases in the amounts of dissolved inorganic carbon and of H<sub>2</sub> that cannot be completely accounted for by production of methane and other small organic molecules, suggesting the possibility that more complex reduced carbon compounds had formed during the experiments. For example, Fu et al. (2007) observed formation of dissolved CO and C<sub>1</sub>-C<sub>3</sub> hydrocarbons during reaction of magnetite with CO<sub>2</sub>- and H<sub>2</sub>-bearing aqueous fluids at 400°C and 50 MPa. Mass balance calculations, however, indicated that ~14% of the inorganic carbon that had been included at the start of the experiments could not be accounted for by the observed products. Those authors suggested that more complex organic compounds had formed, such as longer-chain hydrocarbons. Similarly, in a recently completed series of hydrothermal serpentinization experiments with olivine as the reactant by McCollom et al. (2016), the amounts of H<sub>2</sub> produced during the experiments were up to 20% less than the amounts that should have been generated based on the Fe<sup>III</sup> present in the reaction products. Since only trace amounts of methane and other dissolved organic compounds were observed, these results suggest that some other forms of reduced carbon may be required to account for the “missing” H<sub>2</sub>.

These findings prompted us to investigate the potential for production of insoluble abiotic carbonaceous material during serpentinization. Thermodynamic calculations were performed to explore the ability of carbonaceous material to form and to control the H<sub>2</sub> and CO<sub>2</sub> compositions of aqueous fluids as the serpentinization reaction proceeds. The compositions of experimental and natural fluids reported in the literature are interpreted in the context of these thermodynamic models. The results have implications for diverse geologic

disciplines including global carbon cycling, metamorphic petrology, and subsurface microbiology.

## 2. METHODOLOGY

To place the composition of natural and experimental fluids in a thermodynamic context, equilibrium phase diagrams were constructed for the Fe-O-H-C system. Comparison between fluid compositions and mineral stability domains allows the solid phases expected to precipitate at equilibrium to be identified, and to interpret which phases, if any, might control the fluid composition. The stability domains of minerals involved in the serpentinization reaction were calculated at temperatures from 100 to 400°C and pressures of 35 and 50 MPa using parameters generated with the SUPCRT92 package (Johnson et al., 1992), which incorporates thermodynamic data from Helgeson et al. (1978) for minerals, and Shock and Helgeson (1988) and Shock et al. (1989, 1997) for dissolved inorganic aqueous species.

Predictions of the compositional paths of the fluid and coexisting solids as serpentinization proceeds were calculated with the geochemical code CHES (van der Lee et al., 2002). The CHES software simulates reactions between minerals and fluids, and determines the compositions of minerals and coexisting fluids at thermodynamic equilibrium through minimization of the Gibbs energy of the overall system for a given temperature at steam saturation pressure. By taking into account mass balance, this model allows investigation of constraints on mineral and fluid composition that cannot be studied from activity diagrams alone.

To obtain information on the evolution of fluid compositions during serpentinization of olivine, increments of olivine were added to the models and allowed to react with the fluid while keeping pressure, temperature, and the total amount of fluid constant. We stopped



135 increasing the amount of reacting olivine when a water:olivine mass ratio of  $\sim 2$  was reached,  
136 which is roughly equivalent to the ratio used in number of serpentinization experiments (e.g.,  
137 Berndt et al., 1996; McCollom and Seewald, 2001; Jones et al., 2010). This process simulates  
138 systems where the progress of serpentinization is limited by slow dissolution of olivine while  
139 precipitation of secondary minerals occurs at equilibrium. This assumption appears to be  
140 consistent with laboratory studies of serpentinization under hydrothermal conditions where  
141 olivine is observed to gradually decompose while serpentine, brucite, magnetite and carbonate  
142 minerals precipitate rapidly in apparent equilibrium with the fluid (Berndt et al., 1996;  
143 McCollom and Seewald, 2001; Jones et al., 2010; Malvoisin et al., 2012; McCollom et al.,  
144 submitted).

145         The CHESSE calculations were performed with the LLNL EQ3/6 database version 8  
146 release 6 (e.g., Wolery and Jove-Colon, 2004) and activity coefficients of the aqueous species  
147 were calculated using the truncated-Davies formula (Chandratillake and Robinson, 1990). The  
148 LLNL EQ3/6 database contains equilibrium constants for formation reactions at steam  
149 saturation pressure ( $P_{\text{sat}}$ ). In Figure 1, compositional paths of the fluid are calculated at  $P_{\text{sat}}$   
150 with the CHESSE software and plotted in stability diagrams calculated at elevated pressure (35  
151 MPa) with the SUPCRT92 package. Since pressure has relatively little effect on  
152 thermodynamic equilibria involving condensed phases and dissolved aqueous species, the  
153 differences between the two calculations are low and are neglected herein. Numerous organic  
154 compounds are present by default in the LLNL EQ3/6 database. However, most of these are  
155 not relevant to the model calculations as they are not expected to form at equilibrium with the  
156 fluid due to kinetic limitations. Indeed, formation of methane and most other organic  
157 compounds is known to be highly sluggish at the conditions of serpentinization and  
158 significant formation of methane requires the presence of specific mineral catalysts (Horita  
159 and Berndt, 1999; Seewald et al., 2006). Overall, these compounds represent only a small

fraction of the carbon mass balance during experimental simulation of serpentinization (e.g., Berndt, 1996, McCollom and Seewald, 2001, 2007; Foustoukos and Seyfried, 2004; Seewald et al., 2006). On the other hand, formate and formic acid are expected to rapidly equilibrate with the fluids under serpentinization conditions (McCollom and Seewald, 2003; Seewald et al., 2006). Accordingly, a limited set of organic compounds was included in the models as summarized in Table 1. The organic compounds were chosen based on their stability under the studied serpentinization conditions. Furthermore, some calculations were performed that excluded selected organic species from the equilibrium calculations to test the influence of kinetic limitations on the predicted speciation of carbon compounds (Table 2).

Two different phases of condensed carbonaceous material were considered in the calculations. The stability domains of carbonaceous materials with relatively high organization state (referred to herein as “graphitic carbon”) were calculated by assuming that this phase had thermodynamic properties similar to those of graphite, which is consistent with the experimental results of Milesi et al. (2015). To investigate the possibility that a more hydrogenated phase of condensed carbon forms during serpentinization, anthracene ( $C_{14}H_{10}$ ), a polycyclic aromatic hydrocarbon (PAH) consisting of three fused benzene rings, was adopted as a proxy for this phase in some calculations (referred to herein as “hydrogenated carbon”). Nominally, this compound is intended as a proxy for solid, poorly ordered carbonaceous materials akin to kerogen. Stability domains of various aliphatic and aromatic hydrocarbons were calculated for comparison with that of anthracene (Fig. A1). The low variability between the stability domains supports the use of anthracene as a proxy for a hydrogenated phase of condensed carbon. Thermodynamic data for anthracene are from Richard and Helgeson (1998).

The starting conditions of the reaction path calculations mostly aim to parallel those of the experimental studies of Berndt et al. (1996), McCollom and Seewald (2001) and

McCollom et al. (2016). In the calculations as well as in the experimental studies, the reactant olivine has an Mg-rich composition ( $\sim\text{Fo}_{90}$ ), representative of the chemical composition of this phase in peridotites recovered from the seafloor (Früh-Green et al., 1996, 2004; Mével and Stamoudi, 1996). The input constraints for the reaction path models, including which reduced carbon species are taken into account in each calculation, are listed in Table 2.

Three compositional paths (*Path-1*, -2 and -3) were calculated at 300°C with an aqueous solution containing initially 0.5 mol·L<sup>-1</sup> of NaCl and 20 mmol·L<sup>-1</sup> of NaHCO<sub>3</sub> to provide a source of carbon. This results in dissolved inorganic carbon levels similar to those used in the laboratory experiments, but  $\sim 8\times$  higher than the levels of seawater. At the last increase of the amount of reacting olivine, the water:rock ratio consists of 20 g of olivine for 40 mL of aqueous solution. The three compositional paths differ in the reduced carbon species that are allowed to form at equilibrium with the fluid. In *Path-1*, all organic species listed in Table 1 are considered to equilibrate with the fluid. In *Path-2*, alkanes are excluded from the calculation. In *Path-3*, graphite is removed from the equilibrium system, and no reduced carbon species other than anthracene, carbon monoxide and formic acid are allowed to form. An additional compositional path (*Path-4*) is calculated with similar starting conditions as *Path-2*, but with an initial amount of NaHCO<sub>3</sub> of 100 mmol·L<sup>-1</sup> to ensure saturation with respect to carbonate minerals and allow investigation of the role of carbonate mineral precipitation on fluid composition.

For comparison with the thermodynamic models, activities of dissolved H<sub>2</sub> and CO<sub>2</sub> during laboratory serpentinization experiments and in fluids venting from natural serpentinizing systems were calculated based on measured fluid compositions. The serpentinization experiments considered included those of Berndt et al. (1996), McCollom and Seewald (2001) and McCollom et al. (2016) that initially contained olivine and an aqueous solution containing dissolved inorganic carbon, primarily in the form of bicarbonate

(HCO<sub>3</sub><sup>-</sup>). Experiment #1 of Fu et al. (2007) was conducted at 400°C and 50 MPa with magnetite and an aqueous solution with 170 mmolal of formic acid used as the primary source of dissolved carbon and hydrogen. In addition to consider the measured fluid compositions, H<sub>2(aq)</sub> and CO<sub>2(aq)</sub> compositions in the early stage of the experiment were estimated by assuming a rapid decomposition of the initial amount of 170 mmolal of formic acid according to the reaction:



Experiments of McCollom and Seewald (2003) of decomposition of formic acid in aqueous solution at 250°C and 350 bar showed a rate constant for Reaction (3) of  $1 \cdot 10^{-5}$ , meaning that 90% of the initial amount of formic acid decomposed in ~28 h. Higher decomposition rate are expected at the pressure and temperature conditions of the Fu et al. experiment such that it is reasonable to consider that early H<sub>2(aq)</sub> and CO<sub>2(aq)</sub> concentrations were both ~170 mmol·L<sup>-1</sup> in Experiment #1.

The concentration of total dissolved inorganic carbon is usually expressed as DIC or ΣCO<sub>2(aq)</sub> in the literature (ΣCO<sub>2(aq)</sub> = CO<sub>2(aq)</sub> + HCO<sub>3</sub><sup>-</sup> + CO<sub>3</sub><sup>2-</sup>), and was converted into CO<sub>2</sub> activity for purposes of plotting in phase stability diagrams. The equilibrium speciation of ΣCO<sub>2(aq)</sub> was calculated at the in situ temperature, pressure and pH reported for the experiments or natural fluids using thermodynamic parameters generated with the SUPCRT92 package. Conversion between activity and molality was performed using the activity coefficients calculated with the CHESSE software according to the truncated-Davies model. Neutral species such as dissolved CO<sub>2(aq)</sub> and H<sub>2(aq)</sub> were assumed to have activity coefficients equal to one.

### 3. RESULTS

### 3.1. Reaction path calculations

Calculated mineral stability domains as a function of  $H_{2(aq)}$  and  $CO_{2(aq)}$  activities at 300°C and 35 MPa are shown in Figure 1. Note that olivine is thermodynamically unstable with respect to the other Fe-bearing phases shown in the diagram at this temperature (see McCollom and Bach, 2009). Equilibrium with hydrogenated carbonaceous material as represented by anthracene is achieved for fluid compositions with higher  $H_{2(aq)}$  and  $CO_{2(aq)}$  activities than those required for the formation of graphitic carbon. That is, at the  $H_{2(aq)}$  and  $CO_{2(aq)}$  activities where graphite is predicted to occur in equilibrium with the fluid, hydrogenated carbonaceous material is thermodynamically unstable. The evolution of calculated equilibrium activities of dissolved  $H_{2(aq)}$  and  $CO_{2(aq)}$  during reaction paths for serpentinization of olivine are projected onto the mineral domain in Figure 1. In these calculations, the olivine is incrementally converted to secondary products that include serpentine, brucite and magnetite (plus magnesite in the case of *Path-4*). The carbon speciation, calculated as the percentage of carbon represented by a given species normalized to the total amount of carbon in the system, as well as the fluid pH are plotted as a function of the reaction progress for each of the reaction pathways in Figure 2. At the calculated values of fluid pH, the total concentrations of formate plus formic acid ( $\Sigma HCOOH$ ) and acetate plus acetic acid ( $\Sigma CH_3COOH$ ) are dominated by the anions.

Along each of the reaction paths, the concentration of  $H_{2(aq)}$  increases due to redox reaction between water and ferrous iron in olivine, producing  $H_2$  and ferric iron in magnetite. Concurrently, the  $CO_{2(aq)}$  concentration decreases as reduced carbon species are produced (Fig. 1). In reaction *Path-1*, in which alkanes form at equilibrium with the fluid, essentially all of the initial  $\Sigma CO_{2(aq)}$  is converted to  $CH_4$  (Fig. 2a). When olivine is completely serpentinized at the end of the reaction path, the methane concentration is  $\sim 20 \text{ mmol}\cdot\text{L}^{-1}$  and the  $\Sigma CO_{2(aq)}$  concentration has decreased to  $\sim 1 \text{ nmol}\cdot\text{L}^{-1}$ . Reduced carbon species other than methane are

present in only negligible amounts in the carbon mass balance, although formate is present in amounts representing up to ~1% of the total carbon during intermediate stages of the reaction (Fig. 2a). The pH at reaction conditions is predicted to increase slightly from 8.5 to 8.9 as the reaction progresses.

During reaction *Path-2*, formation of methane and other alkanes is considered to be kinetically inhibited at the reaction conditions of 300°C and 35MPa, as indicated by results of experimental studies (e.g., McCollom and Seewald, 2001; Foustoukos and Seyfried, 2004; Seewald et al., 2006; Fu et al., 2007). At first, the  $H_{2(aq)}$  concentration increases steadily with increasing progress of the serpentinization reaction while the  $CO_{2(aq)}$  concentration remains constant. However, after ~5% of reaction progress, accumulation of  $H_{2(aq)}$  causes the fluid to reach equilibrium with respect to graphitic carbon, which then precipitates and controls the abundance of  $H_{2(aq)}$  and  $CO_{2(aq)}$  in the fluid as serpentinization of olivine proceeds further (Fig. 1a and 2b). The pH values and  $CO_{2(aq)}$  concentrations, relatively constant prior to precipitation of graphitic carbon, increase and decrease, respectively (Fig. 2b). Simultaneously, the rate of  $H_{2(aq)}$  accumulation decreases as it is partially consumed to reduce  $\Sigma CO_{2(aq)}$  into graphitic carbon. Until graphitic carbon begins to precipitate, formate is the dominant reduced carbon compound, and represents up to 6% of the total carbon (Fig. 2b). With continued production of  $H_{2(aq)}$  as serpentinization progresses, increasing amounts of  $\Sigma CO_{2(aq)}$  are converted to graphitic carbon, while formate decreases and is eventually replaced by acetate as the predominant dissolved carbon species. Towards completion of the reaction, dissolved carbon compounds represent increasingly smaller proportion of the total carbon, and by the end of the reaction, graphitic carbon represents ~98% of the total. Other reduced carbon compounds in the model represent only a negligible fraction of the total.

*Path-3* assumes that the most likely solid carbon phase to form during serpentinization would be a partially hydrogenated carbonaceous phase with abundant aromatic moieties,

which is approximated in the calculations by anthracene. Similar to *Path-2*, the  $H_{2(aq)}$  concentration in *Path-3* increases at constant  $CO_{2(aq)}$  concentration during reaction progress until attainment of equilibrium with the hydrogenated carbon phase (Fig. 2c). Then, precipitation of hydrogenated carbon causes the fluid composition to evolve along the  $CO_{2(aq)}$  – hydrogenated carbon equilibrium boundary (Fig. 1a). In this calculation, serpentinization of about 69% of the olivine is required to attain conditions that are sufficiently reducing for the hydrogenated carbon phase to begin to precipitate (Fig. 1a and 2c). Formate is the dominant reduced carbon species all along the reaction path. Its concentration increases up to  $\sim 10 \text{ mmol}\cdot\text{L}^{-1}$  while, concurrently, the pH value decreases slightly before rebounding when the hydrogenated carbon phase starts forming. Once the serpentinization has gone to completion,  $\Sigma CO_{2(aq)}$ ,  $\Sigma HCOOH$  and hydrogenated carbon account for 29, 43 and 28 mol.% of the total carbon, respectively.

Reaction *Path-4* was calculated considering an initially high concentration of  $NaHCO_3$  of  $100 \text{ mmol}\cdot\text{L}^{-1}$ . As in model *Path-2*, the formation of alkanes is assumed to be subject to kinetic limitations (Table 2, Fig. 1b and 2d). In the initial stages of this reaction path, release of  $Mg^{II}$  from olivine leads to precipitation of magnesite rather than brucite, drawing down  $\Sigma CO_{2(aq)}$ . However, after  $\sim 1.4\%$  of reaction, the fluid equilibrates with brucite, allowing both brucite and magnesite to occur in equilibrium (Fig. 1b). While these two phases co-exist, they buffer the  $CO_{2(aq)}$  activity. Generation of  $H_{2(aq)}$  as the reaction progresses leads to saturation of the fluid with respect to graphitic carbon after 2.9% of reaction progress, when this phase begins to precipitate in equilibrium with the fluid (Fig. 1b and 2d). From 2.9 to 19% of reaction, the graphitic carbon – magnesite – brucite assemblage buffers the  $H_{2(aq)}$  and  $CO_{2(aq)}$  composition of the fluid to fixed values (i.e., an invariant point). Eventually, however, carbon reduction leads to conversion of magnesite to graphitic carbon and, once this consumes all of the magnesite, the activities of  $H_{2(aq)}$  and  $CO_{2(aq)}$  are no longer buffered. The fluid

composition evolves along the  $\text{CO}_{2(aq)} - \text{graphitic carbon}$  equilibrium until the olivine is completely serpentinized, similar to that occurring in *Path-2* (Fig. 1b). At the end of the simulation, the solid carbon phase represents 90% of the total carbon. Carboxylic acids are the dominant dissolved organic compounds, representing 4% of the total carbon, with aqueous concentrations of  $\sim 3$  and  $0.6 \text{ mmol}\cdot\text{L}^{-1}$  of  $\Sigma\text{HCOOH}$  and  $\Sigma\text{CH}_3\text{COOH}$ , respectively.

### 3.2. Fluid compositions during experimental studies

Activities of  $\text{H}_{2(aq)}$  and  $\text{CO}_{2(aq)}$  based on measured fluid compositions during laboratory experiments that were intended to simulate conditions during serpentinization are projected onto the mineral stability diagrams shown in Figure 3. In most of the experiments, the abundance of  $\text{H}_{2(aq)}$  increases while  $\text{CO}_{2(aq)}$  decreases as the reactions progress. In the experiments of McCollom and Seewald (2001) and McCollom et al. (2016) at  $300^\circ\text{C}$ , the fluid compositions converge on the equilibrium boundary between  $\text{CO}_{2(aq)}$  and graphitic carbon (Fig. 3b and c). Similar evolution of the fluid composition is observed in the experiments of Fu et al. (2007) and in the McCollom et al. experiments at  $265^\circ\text{C}$ , suggesting that the fluid could be equilibrating with a precipitated insoluble carbonaceous phase (Fig. 3d and e). The decrease of  $\text{H}_{2(aq)}$  in the Fu et al. experiment is due to the fluid composition considered to be initially oversaturated relative to graphitic carbon. In the experiments of Berndt et al. (1996) at  $300^\circ\text{C}$ , the fluid composition converges on equilibrium between  $\text{CO}_{2(aq)}$  and hydrogenated carbon, corresponding to higher  $\text{H}_{2(aq)}$  concentration than the  $\text{CO}_{2(aq)} - \text{graphitic carbon}$  equilibrium (Fig. 3a).

Experiments performed at lower temperatures ( $200\text{--}230^\circ\text{C}$ ) also tend to converge toward equilibrium between  $\text{CO}_{2(aq)}$  and a hydrogenated carbon phase (Fig. 3f and g). In the experiment of McCollom et al. at  $320^\circ\text{C}$ , reaction progress was very limited and the  $\text{H}_{2(aq)}$



concentration remained low. As a consequence, the fluid did not reach the stability domain of graphitic carbon and the  $\text{CO}_2$  concentration is relatively constant (Fig. 3h).

In the experiment of McCollom and Seewald (2001) at  $300^\circ\text{C}$  shown in Figure 3b, the  $\Sigma\text{HCOOH}$  concentrations range from 0.3 to  $0.6 \text{ mmol}\cdot\text{L}^{-1}$ . For similar  $\text{H}_{2(aq)} - \text{CO}_{2(aq)}$  compositions as in this experiment, *Path-2* indicated concentrations of  $\Sigma\text{HCOOH}$  between 0.2 and  $0.9 \text{ mmol}\cdot\text{L}^{-1}$ . These  $\Sigma\text{HCOOH}$  concentrations are also in the same range as those reported in natural serpentinization fluids venting from the Von Damm hydrothermal field on the Mid-Cayman Rise (McDermott et al., 2015), for which temperature and  $\text{H}_{2(aq)} - \text{CO}_{2(aq)}$  fluid composition are comparable.

## 4. DISCUSSION

### 4.1 Condensed carbon in serpentinized rocks

The results of the reaction path models indicate that the formation of solid carbonaceous deposits is thermodynamically favored during serpentinization of ultramafic rocks and can potentially regulate the abundance of  $\text{H}_2$  and the speciation of carbon as the reaction proceeds. However, precipitation of solid carbonaceous materials would require kinetic inhibitions of the formation of methane, since the model *Path-1* allowing attainment of complete thermodynamic equilibrium among all carbon species results in methane becoming the predominant form of carbon (Fig. 2a). The kinetic inhibition of the formation of methane and other light hydrocarbons from the reduction of  $\text{CO}_2$  was argued from many complementary directions long ago and used as a constraint in reaction path calculations (Shock 1990; 1992; Helgeson et al., 1993; Shock and Schulte, 1998). The consequences for the formation of PAHs as a response were predicted for reactions involving volcanic gases (Zolotov and Shock, 1999; 2000) and condensation of the solar nebula (Zolotov and Shock,

2001). Concurrently, a number of laboratory experiments have demonstrated that there are indeed significant kinetic inhibitions to the conversion of dissolved inorganic carbon to methane under hydrothermal conditions at the temperatures where serpentinization occurs (<400 °C) (Berndt et al., 1996; McCollom and Seewald, 2001, 2003, 2007; Foustoukos and Seyfried, 2004; Seewald et al., 2006; McCollom, 2013). In some circumstances, these kinetic inhibitions may be overcome through catalysis by native metal alloys such as awaruite that sometimes precipitate during serpentinization (Horita and Berndt, 1999). Where this does not occur, however, inhibition of methane formation may allow solid carbonaceous matter to form as a metastable equilibrium product of carbon reduction (Fig. 2b-d). In contrast to methane, formation of formate and formic acid at equilibrium with the fluid as suggested by experimental studies (McCollom and Seewald, 2003; Seewald et al., 2006) and natural fluid compositions (Lang et al., 2010; McDermott et al., 2015) does not preclude the fluid from achieving equilibrium with solid carbonaceous material.

It seems likely that any solid carbonaceous matter that precipitates during serpentinization would occur in a disordered, amorphous form rather than as crystalline graphite. Crystalline graphite is generally expected to form only at highly elevated temperatures well above 400°C (e.g., Luque et al., 2009; Beyssac and Rumble, 2014; Rumble, 2014), which is above the temperature range of serpentinization in shallow subsurface environments. Nevertheless, while there are likely to be kinetic inhibitions to formation of crystalline graphite at the temperatures of serpentinization, this would not necessarily preclude equilibrium precipitation of metastable macromolecular reduced carbon phases. For instance, Milesi et al. (2015) observed the formation of solid carbonaceous deposits during experimental dissolution of siderite at temperatures of 200 and 300°C. At 200°C, grains of siderite and magnetite produced during heating were coated by solid carbon whose organization state depended on the mineral surface, while at 300°C solid carbon was found

intimately intermixed with iron oxides at the surface of siderite. Observations of these carbonaceous deposits with a transmission electron microscope (TEM) showed that they were relatively poorly organized carbon phases, except at the surface of magnetites. In addition, regardless of the reaction temperature, a C-bearing phase showing no obvious spatial relationship with mineral phases was found to be highly unstable under the TEM electron beam, suggesting a partially hydrogenated carbonaceous material. In similar siderite decomposition experiments at 300°C, McCollom (2003) reported the formation of polycyclic aromatic hydrocarbons, and the carbonaceous deposits observed by Milesi et al. (2015) may have a large component of aromatic moieties. Consistent with the thermodynamic models considered here, the fluid compositions in the experiments of Milesi et al. (2015) were found to be in agreement with attainment of metastable equilibrium between the fluid and a carbonaceous phase having thermodynamic properties similar to graphite. Carbonaceous materials formed during serpentinization could also be similar to the poorly ordered graphite precipitated from the graphite-undersaturated C – H – O system at 600°C and 1000 MPa reported in experiments by Foustoukos (2012).

Comparison of fluid compositions from laboratory serpentinization experiments with thermodynamic models thus indicates that the experimental results may be consistent with attainment of metastable equilibrium between  $H_{2(aq)}$  and  $\Sigma CO_{2(aq)}$  in the fluid and solid carbonaceous materials having thermodynamic properties similar to graphitic or hydrogenated carbon (Fig. 3). Apart for the experiments of Berndt et al. (1996), all serpentinization experiments at temperature between 265 and 300°C showed fluid composition converging toward the equilibrium boundary between  $CO_{2(aq)}$  and graphitic carbon, which is consistent with model *Path-2* (Fig. 3b, c and e). In the experiments of McCollom et al. (2016) at 300°C, the  $H_2$  production rate is of  $4 \cdot 10^{-3} \text{ mmol} \cdot \text{h}^{-1}$  whereas  $H_2$  was generated at a higher rate of  $1 \cdot 10^{-1} \text{ mmol} \cdot \text{h}^{-1}$  in the experiments of Berndt et al. (1996). This might explain why the experiments

of Berndt et al. (1996) tend to converge toward equilibrium between  $\text{CO}_{2(aq)}$  and hydrogenated carbon, corresponding to higher  $\text{H}_{2(aq)}$  concentrations than the  $\text{CO}_{2(aq)}$  – graphitic carbon equilibrium (Fig. 3a). The higher rate of  $\text{H}_2$  production could be explained by the grain size of the starting olivine of  $< 75 \mu\text{m}$  in the experiments of Berndt et al. (1996) whereas it ranges from 53 to 212  $\mu\text{m}$  in the experiments of McCollom et al. (2016). Fluid compositions of serpentinization experiments performed at lower temperatures (200°C and 230°C) are more consistently described by model *Path-3*. The measured fluid compositions tend to converge toward equilibrium between  $\text{CO}_{2(aq)}$  and hydrogenated carbon rather than graphitic carbon (Fig. 3f and g), which is consistent with the fact that formation of graphitic carbon is generally regarded as a process that occurs at elevated temperatures of 400°C and above (e.g., Luque et al., 2008; Beyssac and Rumble, 2014; Rumble, 2014). In addition to the formation of solid carbonaceous material, precipitation of Mg- and Ca-bearing carbonates contributes to the observed decreases of the  $\text{CO}_{2(aq)}$  activity (McCollom et al., 2016). Owing to the precipitation of unknown amounts of carbonates on the walls of the reaction vessels, it is problematic to calculate an accurate carbon mass balance to estimate the amount that might be converted to carbonaceous materials during serpentinization experiments. However, the amount of  $\text{H}_2$  in many of the experiments is significantly lower than it should be based on the production of ferric Fe in minerals, suggesting the formation of a reduced carbon phase (McCollom et al., 2016).

The observations of Figure 3 suggest that solid carbonaceous materials might have formed in the considered experiments that have so far gone unrecognized. Although there have been no reports to date of the observation of solid carbonaceous deposits among the products of serpentinization experiments, there does not appear to have been any concerted effort to look for such materials among the reaction products. Potentially, carbonaceous products during serpentinization could take the form of either discrete carbon-rich particles or

as thin coatings on the surfaces of mineral phases, similar to those reported by Milesi et al. (2015). In either case, such deposits might be difficult to observe unless specifically targeted for identification.

As indicated by the results of Milesi et al. (2015), the nature of solid carbonaceous precipitates varies with factors such as temperature and the presence of different mineral surfaces, and it seems likely that the variations in conditions between serpentinization experiments could allow for some variation in the types of carbonaceous materials that precipitate, which may explain why some experiments appear to converge towards graphitic carbon while others converge to hydrogenated carbon in the thermodynamic models (Fig. 3). For instance, the  $H_2$  activity of the serpentinization fluids likely has an impact on the nature of the carbonaceous material that precipitates. Sang ely et al. (2007) identified solid bitumen associated with the uranium deposits of Athabasca (Saskatchewan, Canada) that they attributed to the abiotic reduction of  $CO_2$  by  $H_2$  resulting from water radiolysis. Based on isotopic data, the authors proposed that the decrease of  $H_2$  due to the reduction of  $CO_2$  may account for the observed decrease of aliphatic content relative to aromatic content as the solid bitumen accumulates. Zolotov and Shock (2000) evaluate the potential for abiotic synthesis of aliphatic and polycyclic aromatic hydrocarbons from volcanic gas and showed that low  $H/C$  and  $CO/CO_2$  ratio in the gas phase favor the formation of hydrocarbons with high aromatic/aliphatic ratio. Similarly, the aliphatic or aromatic character of hydrocarbons forming from serpentinization fluids may depend on the  $H_{2(aq)}$  and  $CO_{2(aq)}$  compositions of the fluid.

#### *4.2 Natural serpentinization fluids*

Fluid compositions from ultramafic-hosted deep-sea hydrothermal systems also appear to plot near the  $CO_{2(aq)}$  – graphitic carbon boundary, suggesting that equilibration with solid

carbon phases could potentially be taking place during serpentinization in the subsurface (Fig. 4). At high temperatures (300 – 350°C), fluids from the ultramafic-hosted Rainbow, Logatchev, and Von Damm hydrothermal fields are especially close to the stability domain of graphitic carbon (Fig. 4a). In contrast, hydrothermal fluids from basalt-hosted systems, including MARK ½, TAG, Broken Spur, Juan de Fuca and Menez Gwen, appear to be well undersaturated with respect to graphitic carbon, although the Lucky Strike system appears to be close to equilibrium. At lower temperature, fluids from the Lost City hydrothermal system also plot close to the  $\text{CO}_{2(aq)}$  – graphitic carbon equilibrium (Fig. 4c). It is worthwhile to note that when considering a carbon phase that is partially oxygenated and/or contains traces of elements other than carbon that are widespread in serpentinization fluids such as nitrogen, sulfur or silica (Charlou et al., 2002; Foustoukos et al., 2009; Seyfried et al., 2011, 2015; Schrenk et al., 2013), the activity of carbon in the condensed carbon phase would shift to values lower than unity (i.e., activity < 1). This would cause the  $\text{CO}_{2(aq)}$  – condensed carbon equilibrium to shift toward lower  $\text{H}_{2(aq)}$  and  $\text{CO}_{2(aq)}$  activities, equivalent to an increase of the stability domain of the carbon phase, such that the serpentinization fluids would equilibrate with the carbon phase at even lower extents of reaction progress.

These results suggest that precipitation of solid carbonaceous deposits could be playing a role in the reduction of inorganic carbon circulating through actively serpentinizing systems. At present, little evidence has been reported for the occurrence of solid carbonaceous materials within natural serpentinites, although this may be more a reflection of a limited search for such materials than an indication of their absence. Recently, however, Ménez et al. (2012) and Pasini et al. (2013) reported the presence of macromolecular carbonaceous deposits in serpentinites recovered from the seafloor, which the authors attributed to a biological source. Although some aspects of the composition of these deposits could be consistent with a biological origin, the evidence so far has not revealed any property that is

uniquely indicative of a biological origin that would exclude abiotic processes. Consequently, an alternative possibility is that the carbonaceous deposits originated through abiotic reduction of inorganic carbon during serpentinization. Graphite has also been reported to occur in association with several serpentinites, but the source of these deposits remains undetermined (e.g., Krishnarao, 1964; Chidester, 1978; Pasteris, 1981, 1988; Luque et al., 1992, 1998; Miura et al., 2011; Galvez et al., 2013; Kawamoto et al., 2013). Further investigation of these and other types of carbonaceous deposits within serpentinites is required to determine whether solid forms of carbon may be precipitating during serpentinization. The possible occurrence of solid carbonaceous materials in these natural contexts should not be viewed as contradictory with the observation of millimolar levels of abiotic methane in the hydrothermal fluids at some of these locations. As mentioned previously, the production of methane could be favored only at the surface of appropriate, but widely dispersed, minor accessory minerals such as iron-nickel alloys or sulfides (e.g., Horita and Berndt, 1999), resulting in production of small amounts of methane without fully equilibrating with the fluid.

## 5. CONCLUDING REMARKS

Our models show that formation of solid carbonaceous materials from the reduction of  $\text{CO}_{2(aq)}$  is thermodynamically favored during serpentinization of ultramafic rocks, which could potentially regulate the abundance of  $\text{H}_2$  in hydrothermal fluids. Experimental and natural fluid compositions are consistent with attainment of equilibrium between  $\text{CO}_{2(aq)}$  and condensed carbon phases. To date, there have been few reports of the occurrence of solid carbonaceous materials within natural or experimental serpentinites, but the possibility that complex forms of reduced carbon form during serpentinization has received little attention.

Should further investigation of natural systems reveal that solid carbonaceous materials do indeed precipitate from abiotic reduction of inorganic carbon during serpentinization, it would have substantial implications for carbon cycling within the oceanic and continental crust. Any inorganic carbon that is reduced to solid carbonaceous matter would become immobilized, and could potentially be converted to forms that would be recalcitrant to alteration or transport by subsequent processes. Additionally, while methane and other organic compounds formed abiotically in serpentinizing systems are known to support the activities of biological communities, high-molecular-weight carbonaceous materials might be resistant to microbial utilization. In contrast, formation of low-molecular-weight PAHs, such as anthracene or phenanthrene, could represent a food supply for microbes as conditions cool, which could represent a chance for the emergence of heterotrophy in hydrothermal settings. Otherwise, hydrogenated carbonaceous materials might become unstable as conditions change, and continued hydrothermal alteration of these phases could lead to formation of abiotic methane or other organic compounds.

## ACKNOWLEDGMENTS

This work was financially supported by the Institut de Physique du Globe de Paris. T. M.M.'s participation was supported by the Alfred P. Sloan Foundation through the Deep Carbon Observatory. The authors are grateful for the constructive comments of the associate editor Eric Quirico, Everett Shock and two anonymous reviewers. We appreciated stimulating discussions with Alain Prinzhofer and Fabrice Brunet. We especially thank Laurent Richard for his expertise on thermodynamic modeling.

## REFERENCES



528            Berndt M. E., Allen D. E. and Seyfried Jr., W. E. (1996) Reduction of CO<sub>2</sub> during  
529    serpentinization of olivine at 300°C and 500 bar. *Geology* **24**(4), 351-354.

530            Beyssac O., Rouzaud J. N., Goffé B., Brunet F. and Chopin C. (2002) Graphitization  
531    in a high-pressure, low-temperature metamorphic gradient: a Raman microspectroscopy and  
532    HRTEM study. *Contrib. Mineral. Petr.* **143**(1), 19-31.

533            Beyssac O., Brunet F., Petit J. P., Goffé B. and Rouzaud J. N. (2003) Experimental  
534    study of the microtextural and structural transformations of carbonaceous materials under  
535    pressure and temperature. *Eur. J. Mineral.* **15**(6), 937-951.

536            Beyssac O. and Rumble D. (2014) Graphitic carbon: A ubiquitous, diverse, and useful  
537    geomaterial. *Elements*, **10**(6), 415-420.

538            Chandratillake M. R. and Robinson V. J. (1990) Correcting for ionic strength effects in  
539    the Chemval thermodynamic database (EUR-12975) Commission of the European  
540    Communities (CEC)

541            Charlou J. L., Donval J. P., Douville E., Jean-Baptiste P., Radford-Knoery J., Fouquet  
542    Y., Dapoigny A. and Stievenard M. (2000) Compared geochemical signatures and the  
543    evolution of Menez Gwen (37°50'N) and Lucky Strike (37°17'N) hydrothermal fluids, south  
544    of the Azores Triple Junction on the Mid-Atlantic Ridge. *Chem. Geol.* **171**(1), 49-75.

545            Charlou J. L., Donval J. P., Fouquet Y., Jean-Baptiste P. and Holm N. (2002)  
546    Geochemistry of high H<sub>2</sub> and CH<sub>4</sub> vent fluids issuing from ultramafic rocks at the Rainbow  
547    hydrothermal field (36°14'N, MAR). *Chem. Geol.* **191**(4), 345-359.

548            Charlou J. L., Donval J. P., Konn C., Ondréas H., Fouquet Y., Jean-Baptiste P. and  
549    Fourré E. (2010) High production and fluxes of H<sub>2</sub> and CH<sub>4</sub> and evidence of abiotic  
550    hydrocarbon synthesis by serpentinization in ultramafic-hosted hydrothermal systems on the

551 Mid-Atlantic Ridge. *Diversity of hydrothermal systems on slow spreading ocean ridges*, 265-  
552 296.

553 Chidester A. H., Albee A. L. and Cady W. M. (1978) Petrology, structure, and genesis  
554 of the asbestos-bearing ultramafic rocks of the Belvidere Mountain area in Vermont. U.S.  
555 *Geol. Surv. Prof. Paper* 1016.

556 Delacour A., Früh-Green G. L., Bernasconi S. M., Schaeffer P. and Kelley D. S.  
557 (2008) Carbon geochemistry of serpentinites in the Lost City Hydrothermal System (30 N,  
558 MAR). *Geochim. Cosmochim. Ac.* **72**(15), 3681-3702.

559 Etiope G., Tsikouras B., Kordella S., Ifandi E., Christodoulou D. and Papatheodorou  
560 G. (2013a) Methane flux and origin in the Othrys ophiolite hyperalkaline springs, Greece.  
561 *Chem. Geol.* **347**, 161-174.

562 Etiope G., Vance S., Christensen L. E., Marques J. M. and Ribeiro da Costa I. (2013b)  
563 Methane in serpentinized ultramafic rocks in mainland Portugal. *Mar. Petrol. Geol.* **45**, 12-16.

564 Etiope G. and Sherwood Lollar B. (2013) Abiotic methane on Earth. *Rev. Geophys.*  
565 **51**(2), 276-299.

566 Foustoukos D. I. and Seyfried Jr., W. E. (2004) Hydrocarbons in hydrothermal vent  
567 fluids: The role of chromium-bearing catalysts. *Science* **304**(5673), 1002-1005.

568 Foustoukos D. I., Pester N. J., Ding, K. and Seyfried W. E. (2009) Dissolved carbon  
569 species in associated diffuse and focused flow hydrothermal vents at the Main Endeavour  
570 Field, Juan de Fuca Ridge: Phase equilibria and kinetic constraints. *Geochemistry,*  
571 *Geophysics, Geosystems*, **10**(10).

572 Foustoukos D. I. (2012) Metastable equilibrium in the C-H-O system: Graphite  
573 deposition in crustal fluids. *Am. Mineral.* **97**(8-9), 1373-1380.

574 Früh-Green G. L., Connolly J. A. D., Plas A., Kelley D. S. and Grobéty B. (2004)  
575 Serpentinization of Oceanic Peridotites: Implications for Geochemical Cycles and Biological  
576 Activity. In: *The Subseafloor Biosphere at Mid-Ocean Ridges* (Eds. Wilcock W. S. D.,  
577 Delong E. F., Kelley D. S., Baross J. A. and Craig Cary S.) American Geophysical Union,  
578 Washington, D. C.

579 Früh-Green G. L., Plas A. and Lécuyer C. (1996) Petrologic and stable isotope  
580 constraints on hydrothermal alteration and serpentinization of the EPR shallow mantle at Hess  
581 Deep (Site 895). In *Proceedings-Ocean Drilling Program Scientific Results* (255-292).  
582 National Science Foundation.

583 Fu Q., Sherwood Lollar B., Horita J., Lacrampe-Couloume G. and Seyfried Jr., W. E.  
584 (2007) Abiotic formation of hydrocarbons under hydrothermal conditions: Constraints from  
585 chemical and isotope data. *Geochim. Cosmochim. Ac.* **71**(8), 1982-1998.

586 Galvez M. E., Beyssac O., Martinez I., Benzerara K., Chaduteau C., Malvoisin B. and  
587 Malavieille J. (2013) Graphite formation by carbonate reduction during subduction. *Nat.*  
588 *Geosci.* **6**(6), 473-477.

589 Helgeson H. C., Delany J. M., Nesbitt H. W. and Bird D. K. (1978) Summary and  
590 critique of the thermodynamic properties of rock-forming minerals. *Am. J. Sci.* **278A**, 1-229.

591 Helgeson H. C., Knox A. M., Owens C. E. and Shock E. L. (1993) Petroleum, oil field  
592 waters and authigenic mineral assemblages: Are they in metastable equilibrium in  
593 hydrocarbon reservoirs? *Geochim. Cosmochim. Ac.* **57**, 3295-3339.

594 Helgeson H. C. and Shock E. L. (1988) Kinetic and thermodynamic constraints on  
595 phase relations among minerals, petroleum, and aqueous solutions in diagenetic processes.  
596 *Chem. Geol.*, 70(1–2), 78.

597 Holm N. G. and Charlou J. L. (2001) Initial indications of abiogenic formation of  
598 hydrocarbons in the Rainbow ultramafic hydrothermal system, Mid-Atlantic Ridge. *Earth*  
599 *Planet. Sc. Lett.* **191**(1-2), 1-8.

600 Horita J. and Berndt M. E. (1999) Abiogenic methane formation and isotopic  
601 fractionation under hydrothermal conditions. *Science*, **285**(5430), 1055-1057.

602 Johnson J. W., Oelkers E. H. and Helgeson H. C. (1992) SUPCRT92: A software  
603 package for calculating the standard molal thermodynamic properties of minerals, gases,  
604 aqueous species, and reactions from 1 to 5000 bar and 0 to 1000°C. *Comput. Geosci.* **18**(7),  
605 899-947.

606 Jones L. C., Rosenbauer R., Goldsmith J. I. and Oze C. (2010) Carbonate control of H<sub>2</sub>  
607 and CH<sub>4</sub> production in serpentinization systems at elevated P-Ts. *Geophys. Res. Lett.*, **37**,  
608 L14306.

609 Kawamoto T., Yoshikawa M., Kumagai Y., Mirabueno M. H. T., Okuno M. and  
610 Kobayashi T. (2013) Mantle wedge infiltrated with saline fluids from dehydration and  
611 decarbonation of subducting slab. *P. Natl. Acad. Sci. USA*, **110**(24), 9663-9668.

612 Konn C., Charlou J. L., Donval J. P., Holm N. G., Dehairs F. and Bouillon S. (2009)  
613 Hydrocarbons and oxidized organic compounds in hydrothermal fluids from Rainbow and  
614 Lost City ultramafic-hosted vents. *Chemical Geology*, 258(3), 299-314.

615 Konn C., Charlou J. L., Donval J. P. and Holm N. G. (2012) Characterisation of  
616 dissolved organic compounds in hydrothermal fluids by stir bar sorptive extraction-gas

617 chromatography-mass spectrometry. Case study: the Rainbow field (36 N, Mid-Atlantic  
618 Ridge). *Geochem. T.* **13**(8), 1-19.

619 Lang S. Q., Butterfield D. A., Schulte M., Kelley D. S. and Lilley M. D. (2010)  
620 Elevated concentrations of formate, acetate and dissolved organic carbon found at the Lost  
621 City hydrothermal field. *Geochim. Cosmochim. Ac.* **74**(3), 941-952.

622 Luque F. J., Rodas M. and Galán E. (1992) Graphite vein mineralization in the  
623 ultramafic rocks of southern Spain: mineralogy and genetic relationships. *Miner. Deposita*,  
624 **27**(3), 226-233.

625 Luque del Villar F. J., Pasteris J. D., Wopenka B., Rodas M. and Fernández  
626 Barrenechea J. M. (1998) Natural fluid-deposited graphite: mineralogical characteristics and  
627 mechanisms of formation. *Am. J. Sci.* **298**, 471-498.

628 Luque F. J., Ortega L., Barrenechea J. F., Millward D., Beyssac O. and Huizenga J. M.  
629 (2009) Deposition of highly crystalline graphite from moderate-temperature fluids. *Geology*,  
630 **37**(3), 275-278.

631 Malvoisin B., Brunet F., Carlut J., Rouméjon S. and Cannat M. (2012)  
632 Serpentinization of oceanic peridotites: 2. Kinetics and processes of San Carlos olivine  
633 hydrothermal alteration. *J. Geophys. Res. - Sol. Ea. (1978–2012)*, **117**(B4).

634 McCollom T. M. and Seewald J. S. (2001) A reassessment of the potential for  
635 reduction of dissolved CO<sub>2</sub> to hydrocarbons during serpentinization of olivine. *Geochim.*  
636 *Cosmochim. Ac.* **65**(21), 3769-3778.

637 McCollom T. M. (2003) Formation of meteorite hydrocarbons from thermal  
638 decomposition of siderite (FeCO<sub>3</sub>). *Geochim. Cosmochim. Ac.* **67**(2), 311-317.

639 McCollom T. M. and Seewald J. S. (2003) Experimental constraints on the  
640 hydrothermal reactivity of organic acids and acid anions: I. Formic acid and formate.  
641 *Geochim. Cosmochim. Ac.* **67**(19), 3625-3644.

642 McCollom T. M. and Seewald J. S. (2007) Abiotic synthesis of organic compounds in  
643 deep-sea hydrothermal environments. *Chem. Rev.* **107**(2), 382-401.

644 McCollom T. M. and Bach W. (2009) Thermodynamic constraints on hydrogen  
645 generation during serpentinization of ultramafic rocks. *Geochim. Cosmochim. Ac.* **73**(3), 856-  
646 875.

647 McCollom T. M., Klein F., Robbins M., Moskowitz B., Berquó T. S., Jöns N., Bach  
648 W., and Templeton A. (2016) Temperature trends for reaction rates, hydrogen generation, and  
649 partitioning of iron during experimental serpentinization of olivine. *Geochim. Cosmochim.*  
650 *Ac.* **181**, 175-200.

651 McDermott J. M., Seewald J. S., German C. R. and Sylva S. P. (2015) Pathways for  
652 abiotic organic synthesis at submarine hydrothermal fields. *Proc. Natl. Acad. Sci. USA* **112**,  
653 7668-7672.

654 Ménez B., Pasini V. and Brunelli D. (2012) Life in the hydrated suboceanic mantle.  
655 *Nat. Geosci.* **5**(2), 133-137.

656 Mével C. and Stamoudi C. (1996) 15. Hydrothermal alteration of the upper-mantle  
657 section at Hess Deep 1. In: *Proceedings of the Ocean Drilling Program, Scientific Results*  
658 (Eds. Mével C., Gillis K. M., Allan J. F. and Meyer P. S.) Vol. 147

659 Milesi V., Guyot F., Brunet F., Richard L., Reham N., Benedetti M., ... and  
660 Prinzhofer A. (2015) Formation of CO<sub>2</sub>, H<sub>2</sub> and condensed carbon from siderite dissolution in  
661 the 200–300°C range and at 50 MPa. *Geochim. Cosmochim. Ac.* **154**, 201-211.

662 Miura M., Arai S. and Mizukami T. (2011) Raman spectroscopy of hydrous inclusions  
663 in olivine and orthopyroxene in ophiolitic harzburgite: implications for elementary processes  
664 in serpentinization. *J. Miner. Petrol. Sci.* **106**, 91-96.

665 Pasini V., Brunelli D., Dumas P., Sandt C., Frederick J., Benzerara K., ... and Ménez  
666 B. (2013) Low temperature hydrothermal oil and associated biological precursors in  
667 serpentinites from Mid-Ocean Ridge. *Lithos*, **178**, 84-95.

668 Pasteris J. D. (1981) Occurrence of graphite in serpentinized olivines in kimberlite.  
669 *Geology* **9**(8), 356-359.

670 Pasteris J. D. (1988) Secondary graphitization in mantle-derived rocks. *Geology* **16**(9),  
671 804-807.

672 Proskurowski G., Lilley M. D., Seewald J. S., Früh-Green G. L., Olson E. J., Lupton J.  
673 E., Sylva S. P. and Kelley D. S. (2008) Abiogenic hydrocarbon production at Lost City  
674 hydrothermal field. *Science* **319**(8563), 604-607.

675 Rao J. K. (1964) Native nickel-iron alloy, its mode of occurrence, distribution and  
676 origin. *Econ. Geol.* **59**(3), 443-448.

677 Richard L. and Helgeson H. C. (1998) Calculation of the thermodynamic properties at  
678 elevated temperatures and pressures of saturated and aromatic high molecular weight solid  
679 and liquid hydrocarbons in kerogen, bitumen, petroleum, and other organic matter of  
680 biogeochemical interest. *Geochim. Cosmochim. Ac.* **62**(23), 3591-3636.

681 Rumble D. (2014). Hydrothermal graphitic carbon. *Elements*, **10**(6), 427-433.

682 Sangély L., Chaussidon M., Michels R., Brouand M., Cuney M., Huault V. and  
683 Landais P. (2007) Micrometer scale carbon isotopic study of bitumen associated with

684 Athabasca uranium deposits: Constraints on the genetic relationship with petroleum source-  
685 rocks and the abiogenic origin hypothesis. *Earth Planet. Sc. Lett.* **258**(3), 378-396.

686 Schrenk M. O., Brazelton W. J. and Lang S. Q. (2013) Serpentinization, carbon, and  
687 deep life. *Rev. Mineral. Geochem.* **75**, 575-606.

688 Schulte M. D. and Shock E. L. (1993) Aldehydes in hydrothermal solution: Standard  
689 partial molal thermodynamic properties and relative stabilities at high temperatures and  
690 pressures. *Geochim. Cosmochim. Ac.* **57**, 3835-3846.

691 Seewald J. S., Zolotov M. Y. and McCollom T. (2006) Experimental investigation of  
692 single carbon compounds under hydrothermal conditions. *Geochim. Cosmochim. Ac.* **70**(2),  
693 446-460.

694 Seyfried W. E., Pester N. J., Ding K. and Rough M. (2011) Vent fluid chemistry of the  
695 Rainbow hydrothermal system (36 N, MAR): Phase equilibria and in situ pH controls on  
696 seafloor alteration processes. *Geochim. Cosmochim. Ac.* **75**(6), 1574-1593.

697 Shilobreeva S., Martinez I., Busigny V., Agrinier P. and Laverne C. (2011) Insights  
698 into C and H storage in the altered oceanic crust: Results from ODP/IODP Hole 1256D.  
699 *Geochim. Cosmochim. Ac.* **75**(9), 2237-2255.

700 Shock E. L. (1990) Geochemical constraints on the origin of organic compounds in  
701 hydrothermal systems. *Origins Life Evol. B.* **20**, 331-367.

702 Shock E. L. (1992) Chemical environments in submarine hydrothermal systems. In:  
703 *Marine Hydrothermal Systems and the Origin of Life*, (ed. N. Holm) a special issue of *Origins*  
704 *Life Evol. B.* **22**, 67-107.



705 Shock E. L. (1995) Organic acids in hydrothermal solutions: Standard molal  
706 thermodynamic properties of carboxylic acids and estimates of dissociation constants at high  
707 temperatures and pressures. *Amer. Jour. Sci.* **295**, 1255-1342.

708 Shock E. L. and Helgeson H. C. (1990) Calculation of the thermodynamic and  
709 transport properties of aqueous species at high pressures and temperatures: Standard partial  
710 molal properties of organic species. *Geochim. Cosmochim. Ac.* **54**, 915-945.

711 Shock E. L., Helgeson H. C. and Sverjensky D. A. (1989) Calculation of the  
712 thermodynamic and transport properties of aqueous species at high pressures and  
713 temperatures: Standard partial molal properties of inorganic neutral species. *Geochim.*  
714 *Cosmochim. Ac.* **53**, 2157-2183.

715 Shock E. L. and McKinnon W. B. (1993) Hydrothermal processing of cometary  
716 volatiles - Applications to Triton. *Icarus*, **106**, 464-477.

717 Shock E. L., Sassani D. C., Willis M., and Sverjensky D. A. (1997) Inorganic species  
718 in geologic fluids: Correlations among standard molal thermodynamic properties of aqueous  
719 ions and hydroxide complexes. *Geochim. Cosmochim. Ac.* **61**, 907-950.

720 Shock E. L. and Schulte M. D. (1998) Organic synthesis during fluid mixing in  
721 hydrothermal systems. *J. Geophys. Res.* **103**(E12), 28513–28527

722 van Der Lee J., De Windt L., Lagneau V. and Goblet P. (2002) Presentation and  
723 application of the reactive transport code HYTEC. *Dev. Water Sci.* **47**, 599-606.

724 van Zuilen M. A., Lepland A., Teranes J., Finarelli J., Wahlen M. and Arrhenius G.  
725 (2003) Graphite and carbonates in the 3.8 Ga old Isua Supracrustal Belt, southern West  
726 Greenland. *Precambrian Res.* **126**(3-4), 331-348.

727           Wolery, T. J., and C. F. Jove-Colon (2004) Qualification of thermodynamic data for  
728   geochemical modeling of mineral–water interactions in dilute systems. U.S. Department of  
729   Energy, Las Vegas, Nevada.

730           Zolotov M. Y. and Shock E. L. (1999) Abiotic synthesis of polycyclic aromatic  
731   hydrocarbons on Mars. *Jour. Geophys. Res.* **104**, 14033-14049.

732           Zolotov M. Y. and Shock E. L. (2000) A thermodynamic assessment of the potential  
733   synthesis of condensed hydrocarbons during cooling and dilution of volcanic gases. *Jour.*  
734   *Geophys. Res.* **105**, 539-559.

735           Zolotov M. Y. and Shock E. L. (2001) Stability of condensed hydrocarbons in the solar  
736   nebula. *Icarus* **150**, 323-337.

**Table 1.** Reduced carbon species considered in the modeling

Compounds	Formula	Reference-state data source*
Methane	CH <sub>4</sub>	Shock and Helgeson (1990)
Ethane	C <sub>2</sub> H <sub>6</sub>	Shock and Helgeson (1990)
Ethylene	C <sub>2</sub> H <sub>4</sub>	Shock and Helgeson (1990)
Formate	HCOO <sup>-</sup>	Shock (1995)
Formic acid	HCOOH	Shock (1995)
Acetate	CH <sub>3</sub> COO <sup>-</sup>	Shock (1995)
Acetic acid	CH <sub>3</sub> COOH	Shock (1995)
Formaldehyde	HCOH	Schulte and Shock (1993)
Acetaldehyde	CH <sub>3</sub> COH	Schulte and Shock (1993)
Methanol	CH <sub>3</sub> OH	Shock and Helgeson (1990)
Ethanol	C <sub>2</sub> H <sub>5</sub> OH	Shock and Helgeson (1990)
Carbon monoxide	CO	Shock and McKinnon (1993)
Graphite	C	Helgeson et al. (1978)
Anthracene	C <sub>14</sub> H <sub>10</sub>	Richard and Helgeson (1998)

\* The thermodynamic properties of the selected reduced carbon species at high temperatures (0 – 300°C) in the LLNL EQ3/6 database are calculated with the SUPCRT92 software package (Johnson et al., 1992).

**Table 2.** Starting conditions of reaction path calculations

Reaction path	$\Sigma\text{CO}_2$ (mmol·L <sup>-1</sup> )	Reduced carbon species included
<i>Path-1</i>	20	All reduced species reported in Table 1
<i>Path-2</i>	20	Alkanes excluded; all other reduced species included
<i>Path-3</i>	20	Anthracene, CO <sub>(aq)</sub> , HCOOH, and HCOO <sup>-</sup> only
<i>Path-4</i>	100	Alkanes excluded; all other reduced species included

## FIGURE CAPTIONS

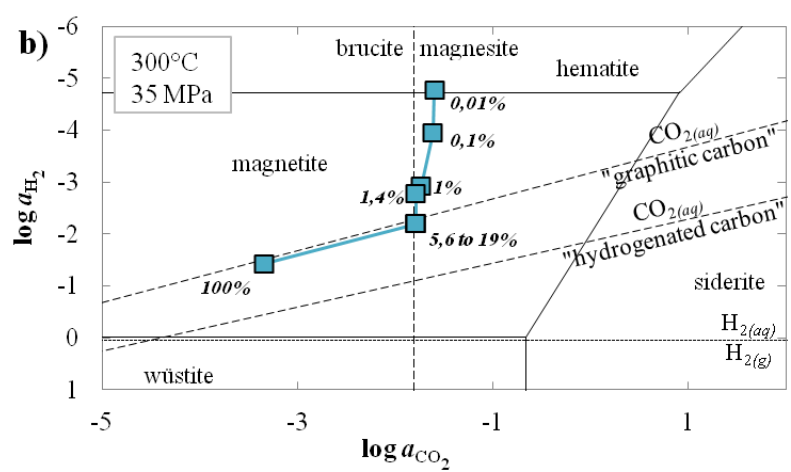
**Figure 1.** Calculated  $\text{H}_2 - \text{CO}_2$  composition of fluids during serpentinization of olivine projected onto solid phase stability domains in the Fe-Mg-O-C-H system as a function of  $\text{H}_2$  and  $\text{CO}_2$  activities at 300°C and 35 MPa. *Path-1* (red full circles), 2 (blue full squares) and 3 (green full diamonds) are plotted in diagram (a), and *Path-4* (blue full squares) in diagram (b). The percentages near the symbols indicate the progress of the serpentinization reaction (i.e., the amount of olivine reacted). The concentration corresponding to saturation of the fluid with respect to  $\text{H}_2$  gas is represented by the grey, short-dashed horizontal line. Note that the activity of  $\text{H}_2$  increases going downward in the figure.

**Figure 2.** Carbon speciation, calculated as the percentage of carbon in a given species relative to the total amount of carbon in the system, and pH at reaction conditions as a function of the reaction progress (i.e., the percentage of olivine serpentinized). Panels a, b, c and d correspond to *Path-1*, 2, 3 and 4, respectively.

**Figure 3.** Fluid compositions from serpentinization and related experiments projected onto  $\text{H}_2 - \text{CO}_2$  activity diagrams. Experimental data are from Berndt et al. (1996) (box a, yellow triangles), McCollom and Seewald (2001) (box b, orange diamonds and circles), Fu et al. (2007) (box d, blue squares) and McCollom et al. (2016) (box c, e, f, g and h; blue, purple, light green, green and light blue diamonds, respectively). The arrows show the reaction progress.

**Figure 4.** End-member fluid compositions for deep-sea hydrothermal systems and terrestrial serpentinite springs projected onto  $H_2 - CO_2$  activity diagrams. For clarity, the plotted  $H_2$  and  $CO_2$  composition of the Juan de Fuca hydrothermal fluids corresponds to the average value of six homogeneous end-member compositions (see Foustoukos et al., 2009). For the Lost City hydrothermal field, several end-member fluid compositions are plotted from different sample sites (see Proskurowski et al., 2008, supporting online material) and a pH value of 9 is considered for calculation of the DIC speciation. Measured temperatures for the hydrothermal fluids shown in (a) and (b) are in the 300-350°C range, although peak temperatures in subsurface reaction zones may be somewhat higher. Although vent temperatures at Lost City are ~90°C, temperatures in the subsurface reaction zones where these fluids originate is thought to be 150-200°C (Proskurowski et al., 2006; Foustoukos et al., 2008). Since pressure has little effect on thermodynamic equilibria, all diagrams are calculated at 35MPa. Data sources: Rainbow (2), Logatchev, MARK1/2, TAG, Broken Spur (box *a*): Charlou et al. (2002) and references therein; Rainbow (1) (box *a*): Seyfried et al. (2011); Juan de Fuca (box *a*): Foustoukos et al. (2009); Menez Gwen, Lucky Strike (box *b*): Charlou et al. (2000); Von Damm (box *b*): McDermott et al. (2015); Lost City (box *c*): Proskurowski et al. (2008).

**Figure A1.** Stability domains of “graphitic carbon”, aliphatic and aromatic hydrocarbons as function of  $H_2$  and  $CO_2$  activities. Thermodynamic properties for aliphatic and aromatic hydrocarbons are from Richard and Helgeson (1998).



Revised Figure 2

